Biophysical Chemistry 28 (1987) 35–50
Elsevier

BPC 01181

Analysis of fluorescence decay kinetics measured in the frequency domain using distributions of decay times

Joseph R. Lakowicz [a], Henryk Cherek [a,*], Ignacy Gryczynski [a,**], Nanda Joshi [a] and Michael L. Johnson [b]

[a] *University of Maryland, School of Medicine, Department of Biological Chemistry, 660 West Redwood Street, Baltimore, MD 21201 and* [b] *University of Virginia, Department of Pharmacology, Charlottesville, VA 22908, U.S.A.*

Received 20 April 1987
Accepted 8 June 1987

Fluorescence decay; Decay-time distribution; Kinetics; Frequency-domain fluorometry

We describe the theoretical and practical aspects of analyzing complex fluorescence decay kinetics using continuous distributions of decay times. Our analysis uses frequency-domain data, provides for global analysis of multiple data sets and includes the possibility of excited-state processes. Simulated data were used to estimate the types of distributions which can be reasonably recovered from the measurements. Additionally, we describe a variety of distributions recovered from experimental data. For mixtures of one, two or three exponentially decaying fluorophores we recovered narrow lifetime distributions, which are essentially identical to a multiexponential decay. Similarly, a two-state excited-state reaction also yielded a narrow distribution with negative preexponential factors. The presence of time-dependent spectral relaxation of labeled lipids results in a wide distribution of decay times, which becomes narrower for faster relaxation rates at higher temperatures. Hence, the decay-time distributions appear to be sensitive to the dynamics of the environment surrounding the fluorophore. Additionally, distributions of decay times were observed to result from transient effects in collisional quenching, from energy transfer in the presence of a range of donor-to-acceptor distances, and for several single-tryptophan proteins.

1. Introduction

The application of fluorescence spectroscopic methods to biochemical samples often involves analysis of the intensity decay kinetics. The decay times or lifetimes are of interest because they can represent molecular features of the sample, such as the presence of two or more tryptophan residues in a protein, the existence of two or more conformations or the occurrence of an excited-state reaction. During the past decade it has become common practice to analyze intensity decays using a sum of discrete exponential decays [1–4], possibly because of the intuitive association of the individual decay times with discrete emitting species. This practice has provided the easiest route to interpreting the recovered parameters. Also, the multiexponential model provides an adequate number of parameters to account for the data with the limited resolution of the time-resolved data.

In the present report we describe the analysis of

Correspondence address: J.R. Lakowicz, University of Maryland, School of Medicine, Department of Biological Chemistry, 660 West Redwood Street, Baltimore, MD 21201, U.S.A.

* Permanent address: Nicholas Copernicus University, Torun, Poland.

** Permanent address: Institute of Experimental Physics, University of Gdansk, Poland.

Abbreviations: Gau, Gaussian distribution; Het, heterogeneous distribution or multiexponential model; Lor, Lorentzian distribution; ANT, anthracene; DOPC, dioleoyl-L-α-phosphatidylcholine; fw, full-width at half-maximum; POPOP, *p*-bis[2-(5-phenyloxazolyl)]benzene; TNS, 2-*p*-toluidinyl-t-naphthalenesulfonic acid; 9-CA, 9-cyanoanthracene; 9-MA, 9-methylanthracene; 9-VA, 9-vinylanthracene; 9,10-DMA, 9,10-dimethylanthracene; RNase T_1, ribonuclease T_1.

intensity decay kinetics using a alternative model, which allows for a continuous distribution of decay times. Lifetime distributions have been the subject of several recent publications [5–10], and to some extent these papers reflect an extension of the earlier analysis of decay kinetics using a series of equally spaced exponentials [11]. Some early reports indicated that the data obtained using time-correlated single-photon counting may not be adequate to recover the lifetime distributions [6,7]. However, the situation may be improving as the result of the more widespread use of pulse picosecond lasers for time-correlated single-photon counting, which provides a higher number of counts and hence higher statistical accuracy [4,7,12,13], and because of the recent development of frequency-domain fluorometers [14–16].

In the present paper we describe simulations which illustrate the resolution which can be expected from the frequency-domain data. The analysis methods were verified using data from mixtures of fluorophores. The theory was applied to systems where one expects the decays to be more correctly described by lifetime distributions. These systems included samples which displayed time-dependent spectral shifts [17,18], transient effects in quenching [19–22], energy transfer to multiple acceptors at different distances [23–25], and the emission from several single-tryptophan proteins. The effects of time-dependent shifts are of particular interest because the lifetime distributions could reveal the dynamic properties of the environment which surrounds the fluorophore.

2. Theory

Fluorescence intensity decays are usually described as the sum of individual exponentials. The intensity decay following δ-function excitation is described by

$$I(t) = \sum_i \alpha_i e^{-t/\tau_i} \tag{1}$$

where τ_i are the individual decay times and α_i the associated preexponential factors. The fractional contribution of the i-th component to the total emission is

$$f_i = \frac{\alpha_i \tau_i}{\sum_i \alpha_i \tau_i}, \tag{2}$$

It is common practice to normalize the α_i and f_i values so that $\Sigma\alpha_i = 1.0$ and $\Sigma f_i = 1.0$.

We now consider an alternative model in which the α_i values are not discrete amplitudes at τ_i, but rather are described by a continuous distribution $\alpha(\tau)$. The intensity decay then contains components of each lifetime τ with an amplitude $\alpha(\tau)$. The component with each individual τ value is given by

$$I(\tau, t) = \alpha(\tau) e^{-t/\tau}. \tag{3}$$

The total decay law is the sum of the individual decays weighted by the amplitudes,

$$I(t) = \int_{\tau=0}^{\infty} \alpha(\tau) e^{-t/\tau}\, d\tau \tag{4}$$

where $\int \alpha(\tau)\, d\tau = 1.0$. The relationship between the two models (eqs. 1 and 4) can be seen by considering $\alpha(\tau)$ to be a δ-function centered at $\tau = \tau_0$, i.e., $\alpha(\tau) = \delta(\tau - \tau_0)$. Then, using the properties of the δ-function,

$$I(t) = \int_{\tau=0}^{\infty} \delta(\tau - \tau_0) e^{-t/\tau}\, d\tau = e^{-t/\tau_0} \tag{5}$$

Hence, a δ-function distribution of $\alpha(\tau)$ is equivalent to a single-exponential decay. One can expand $\alpha(\tau)$ to include several α-weighted δ-functions. Then, application of eq. 5 yields the multi-exponential decay law.

At present we do not have a theoretical model to predict the $\alpha(\tau)$ distributions, nor do we have adequate experience or experimental results to choose a particular distribution function. Hence, we arbitrarily selected Gaussian (G) and Lorentzian (L) lifetime distributions. For these functions the $\alpha(\tau)$ values are

$$\alpha_G(\tau) = \frac{1}{\sigma\sqrt{2\pi}} \cdot e^{-\frac{1}{2}\left(\frac{\tau-\bar{\tau}}{\sigma}\right)^2} \tag{6}$$

$$\alpha_L(\tau) = \frac{1}{\pi} \cdot \frac{\Gamma/2}{(\tau-\bar{\tau})^2 + (\Gamma/2)^2} \tag{7}$$

where $\bar{\tau}$ is the central value of the distribution, σ

the standard deviation of the Gaussian, and Γ the full-width at half-maximum (fw) for the Lorentzian. For a Gaussian the full-width at half-maximum is given by 2.354σ [26]. For ease of interpretation we describe both distributions by the full-width at half-maxima. An alternative approach would be to use $\alpha(\tau)$ distributions which are not described by any particular function. This approach may be superior in that it makes no assumptions about the shape of the distribution. However, the use of functional forms for $\alpha(\tau)$ minimizes the number of floating parameters in our fitting algorithms.

By analogy with the multiexponential model, it seems probable that $\alpha(\tau)$ could be multimodal. Then

$$\alpha(\tau) = \sum_i g_i \alpha_i^0(\tau) = \sum_i \alpha_i(\tau) \tag{8}$$

where i refers to the i-th component of the distribution centered at $\bar{\tau}_i$, and g_i represents the amplitude of this component. The g_i values are the amplitude factors and $\alpha_i^0(\tau)$ the shape factors describing the distribution. We used normalized expressions (eqs. 6 and 7) for the individual $\alpha_i^0(\tau)$ so that $\int \alpha_i^0(\tau)\, d\tau = 1.0$ when there is no α density below $\tau = 0$.

It is important to recognize the meaning of the terms in eq. 8. For distributions with no significant amplitude near the origin the amplitude factors (g_i) are analogous to the α_i values in eq. 1. This can be seen by recalling that the $\alpha_i^0(\tau)$ are normalized. Hence,

$$\int_0^\infty \alpha_i(\tau)\, d\tau = \int_0^\infty g_i \alpha_i^0(\tau)\, d\tau = g_i \tag{9}$$

However, there may be $\alpha(\tau)$ density near or below the $\tau = 0$ origin, especially when one remembers that such density represents small fractional contributions to the total emission (eq. 2), and that the density below $\tau = 0$ has no physical significance. In this case the individual $\alpha_i^0(\tau)$ distributions are not normalized, and the g_i values do not represent the normalized amplitude of each component. For example, consider a component centered at $\tau = 0$ so that only one-half of $\alpha_i(\tau)$ is relevant. Then, the integrated amplitude of $\alpha_i(\tau)$ would not be properly normalized. For consistency, we define $\alpha_i(\tau)$ as the integrated preexponential factor for each component. For any distribution, including those cut off at the origin,

$$\alpha_i = \frac{\int_0^\infty \alpha_i(\tau)\, d\tau}{\int_0^\infty \sum_i \alpha_i(\tau)\, d\tau} \tag{10}$$

The fractional contribution of the i-th component to the total emission is given by

$$f_i = \frac{\int_0^\infty f_i(\tau)\tau\, d\tau}{\int_0^\infty \sum_i f_i(\tau)\tau\, d\tau}. \tag{11}$$

2.1. Excited-state reactions

An excited-state reaction yields an emitting species which is distinct from the initially excited state. Such processes include loss of protons in the excited state [27], excimer formation [28] and solvent reorganization [29,30]. Examination of the $\alpha(\tau)$ distributions should be particularly informative in such cases. Suppose one obtains data across the emission spectrum. The form of the intensity decay depends upon the reversibility of the reaction, and the species responsible for the emission at each wavelength [27–34]. Typically, the decay is complex on the red and blue sides of the emission, and a single exponential at one wavelength near the center. The lifetime distributions should reflect this complex behavior. Analysis of the fluorescence data from such systems is more complicated in both the time [27,31] and frequency domains [32–34]. An excited-state process results in a negative preexponential factor in the time domain (eq. 1). To keep the time-resolved intensity positive, and hence rational, the longer decay time must be associated with the positive preexponential factor. Importantly, the amplitudes no longer represent the contributions of the individual components, as these cannot be negative. Calculation of the integrated α_i values (eq. 11) is also complicated because the α_i values from eq. 1 or 10 can be equal and opposite. Hence, $\int \alpha(\tau)\, d\tau$ can be near or equal to zero. In this case one must use eq. 10

or 11 with the absolute values of each integral in the denominator. This yields values for α_i and f_i, but their significance is not obvious without more detailed analysis.

2.2. Frequency-domain theory for lifetime distributions

The frequency response of the emission consists of the frequency-dependent values of the phase angle (ϕ_ω) and the demodulation factor (m_ω), where ω refers to the modulation frequency in rad/s. These values can be calculated from the sine (N_ω) and cosine (D_ω) transforms of the impulse response function. Using eq. 4 these transforms are

$$N_\omega J = \int_{t=0}^{\infty}\int_{\tau=0}^{\infty} \alpha(\tau) e^{-t/\tau}\, d\tau \sin \omega t\, dt \qquad (12)$$

$$D_\omega J = \int_{t=0}^{\infty}\int_{\tau=0}^{\infty} \alpha(\tau) e^{-t/\tau}\, d\tau \cos \omega t\, dt. \qquad (13)$$

Reversal of the order of integration yields

$$N_\omega J = \int_{\tau=0}^{\infty} \frac{\alpha(\tau)\omega\tau^2}{1+\omega^2\tau^2} d\tau \qquad (14)$$

$$D_\omega J = \int_{\tau=0}^{\infty} \frac{\alpha(\tau)\tau}{1+\omega^2\tau^2} d\tau \qquad (15)$$

with

$$J = \int_{\tau=0}^{\infty} \alpha(\tau)\tau\, d\tau. \qquad (16)$$

For any parameter values the calculated (c) phase and modulation values are

$$\phi_{c\omega} = \arctan(N_\omega/D_\omega) \qquad (17)$$

$$m_{c\omega} = \left(N_\omega^2 + D_\omega^2\right)^{1/2} \qquad (18)$$

3. Methods

3.1. Analysis of the frequency-domain data

The measured phase (ϕ_ω) and modulation values (m_ω) were analyzed by the method of nonlinear least squares [35,36]. Calculated values were obtained using eqs. 12–18. The goodness-of-fit was judged by the value of reduced χ^2

$$\chi_R^2 = \frac{1}{\nu}\sum_{\omega,k}\left(\frac{\phi_\omega - \phi_{c\omega}}{\delta\phi}\right)^2 + \frac{1}{\nu}\sum_{\omega,k}\left(\frac{m_\omega - m_{c\omega}}{\delta m}\right)^2 \qquad (19)$$

where ν is the number of degrees of freedom, and $\delta\phi$ and δm the uncertainties in the measured phase and modulation values, respectively. In eq. 19 the sum extends over all frequencies (ω), and in some cases over multiple sets of data or multiple emission wavelengths (k). For instance, we examined mixtures of fluorophores with varying proportions of the individual fluorophores. The lifetimes were constrained to be constant for all files, but the amplitudes (α_i and f_i) varied for each file. This global method was described previously in more detail for time- [37] and frequency-domain data [35]. An example may clarify this concept. We examined five different mixtures of 9-MA and 9-CA, which included data at about 15 frequencies per mixture, for a total of 150 data points. The data were analyzed with two mean decay times which were variable, but the same for all mixtures. The bimodal Gaussian model has nine floating parameters (two lifetimes, two full-widths, and one amplitude per file, since $\Sigma\alpha_i = 1.0$). Hence, this global analysis has 141 degrees of freedom.

Our analysis programs are written in both Basic-11 and Fortran 77 for Dec 11/73 computers. These programs use the Gauss-Newton and Marquardt-Levenburg methods of nonlinear least squares [26,35]. The integrals are calculated numerically. The uncertainty estimates include correlation between the parameters [38]. Simulations were performed as described previously [35]. Typically, the data were simulated for about 20 frequencies, distributed approximately equally on the log frequency scale. Gaussian noise was added to the simulated data using $\delta\phi = 0.2^0$ and $\delta m = 0.005$, which are approximately equal to the experimental values.

The frequency-domain data were measured using the instruments described previously [15,16], under the specific conditions listed in the text. The data for the labeled DOPC vesicles were from an earlier study of time-resolved emission spectra [39].

The data for acrylamide-quenched indole and for the donor-acceptor pair are also from previous reports [25,40].

4. Results and discussion

4.1. Effects of a lifetime distribution on the frequency response

It is of interest to examine the effect of a lifetime distribution on the frequency-domain data. Representative Lorentzian distributions are shown in fig. 1 for unimodal (top) and bimodal (bottom) cases. It is important to note that the Lorentzian curve for fw = 5 has greater amplitude at lifetime values outside the fw, whereas the Gaussian curve decays more rapidly to zero. The Gaussian distribution has over 98% of its area within ±one half-width (fw/2). In contrast, the Lorentzian contains only 71% of its area within ±2 half-widths. To account for 99% of the area of a Lorentzian one must use ±62 half-widths. This is an important distinction, which has a dramatic effect on the full-widths recovered from the analysis. For a single-exponential decay (fw = 0) the apparent widths recovered from the Lorentzian model are smaller because the smaller width suppresses the tails of the distribution. We used simulated data with the distribution from fig. 1 to estimate the resolution possible with the frequency-domain data.

After a number of simulations and experimental studies we conclude that it is rather difficult to distinguish a distribution from a multiexponential decay. To be more specific, it is difficult to distinguish a unimodal distribution from a double-exponential decay or a bimodal distribution from a triple-exponential decay. This is illustrated for the unimodal case in fig. 2, which shows simulated data for $\bar{\tau}$ = 15 ns and fw = 5 ns. The data contain random noise at a level comparable to our experimental data. We attempted to fit the simulated data to a single-exponential decay. This fit was unacceptable, as indicated by the large value of

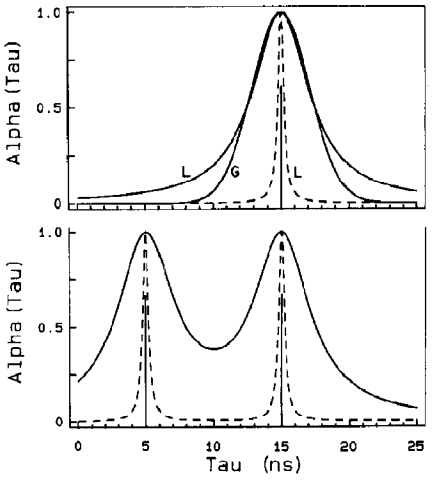

Fig. 1. Unimodal (top) and bimodal (bottom) distributions of decay times. (Top) $\bar{\tau}$ = 15 ns; fw = 5 ns for a Lorentzian (L) or a Gaussian (G); fw = 0.5 ns for a Lorentzian (— — —); The vertical bar is for a single-exponential decay, fw = 0.0. (Bottom) $\bar{\tau}$ = 5 ns, $\bar{\tau}_2$ = 15 ns; $fw_1 = fw_2$ = 5 ns (———) or $fw_1 = fw_2$ = 0.5 ns (- - - - -) for a bimodal Lorentzian. Also shown is a double-exponential decay (vertical bars).

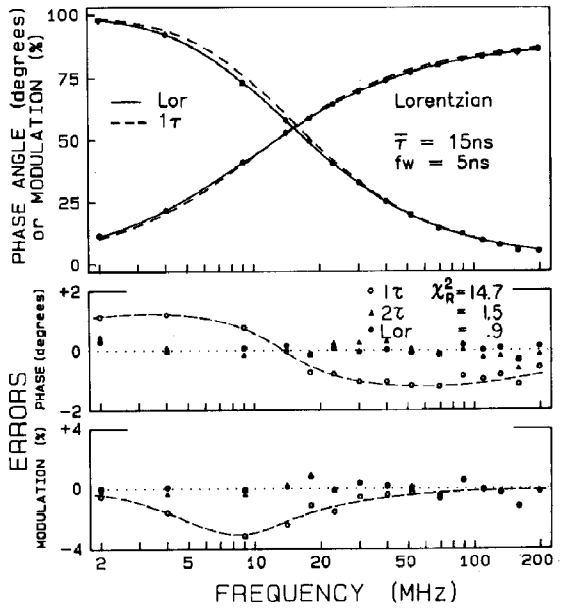

Fig. 2. Effect of a Lorentzian distribution of decay times on the frequency-domain data. The best fit with fw = 0.0 (— — —, ○) yields χ^2_R = 14.7. The correct parameter values are recovered ($\bar{\tau}$ = 15 ns, fw = 5 ns, χ^2_R = 0.90) when $\bar{\tau}$ and fw are variable, and the deviations are smaller and more random (lower panels, ●). The deviations (△) for a two-component decay are also small and randomly distributed; χ^2_R = 1.5.

$\chi^2_R = 14.7$ and the systematic deviations between the simulated and calculated values (O, lower panels). Although not evident from the figure, the effect of a lifetime distribution is to increase the width of the frequency response. However, the difference between the expected values for a full-width of 5 ns (———) and for a full-width of 0.0 ns (— — —) is not dramatic. This may be the result of partial cancellation of the contribution of components above and below the mean value of τ. From examination of a number of simulated files we know that the correct values for the parameters ($\bar{\tau} = 15$ ns, fw = 5 ns) can be recovered from the simulated data. For this model the deviations are randomly distributed (fig. 2, lower panel) and $\chi^2_R = 0.90$. However, without additional information it would be difficult to distinguish the data from those due to a double-exponential decay. For this model the deviations are again randomly distributed (△) and $\chi^2_R = 0.15$.

4.2. Detection of lifetime distribution

An important question is whether one can distinguish a distribution of lifetimes from a sum of exponentials. This is a complex question, which we cannot answer in a general way. For any set of data the ability to recover the correct parameters is a complex function of the parameter values, correlation between the parameters, number of data points and their significance, and the extents of random and nonrandom error. Additionally, the recovered parameters will only be meaningful if the model is correct. At present we do not believe that it is possible to distinguish distributions with similar shapes on the basis of the values of χ^2_R or the appearance of the residuals, such as a Gaussian or a skewed Gaussian. Hence, we describe a series of simulations which broadly define whether a particular distribution can be distinguished from a multiexponential model based on the values of χ^2_R.

Frequency-domain data were simulated for unimodal and bimodal distributions (fig. 3, left and right, respectively). We used the distributions shown in fig. 1, with $\bar{\tau} = 15$ ns for the unimodal case and $\bar{\tau} = 5$ and 15 ns for the bimodal distribution. The full-width of the simulated data was

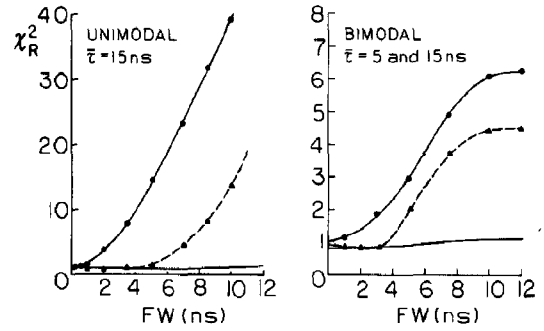

Fig. 3. Dependence of χ^2_R from the multiexponential model on the widths of lifetime distributions. (●) Multiexponential fits to the Lorentzian distributions; (▲) fits to the Gaussian distributions. The lines near $\chi^2_R = 1$ represent the two-component fits to the unimodal distributions (left) and the three-component fits to the bimodal distribution. (Left) $\bar{\tau} = 15$ ns; (right) $\bar{\tau}_1 = 5$ ns, $\bar{\tau}_2 = 15$ ns, $f_1 = f_2 = 0.5$.

increased as indicated by the x-axes. The simulated data were then analyzed with the single- (left) or double-exponential model (right), which has a full-width of zero. To aid in interpreting the values of χ^2_R we note that with 25 degrees of freedom a 2-fold increase in χ^2_R is adequate to state with 99.9% certainty that the model is not adequate to account for the data.

If the decay is known to be unimodal then it is relatively easy to determine whether a distribution is present (fig. 3, left). For a Lorentzian distribution (●) a full-width of 2 ns yields $\chi^2_R = 4$, which is easily adequate to reject the single-exponential model. The value of χ^2_R exceeds 2 for a full-width of about 1 ns. The χ^2_R surface is smooth and local minima were not usually encountered. The situation is less favorable for a Gaussian distribution (▲). In this case χ^2_R does not increase above 2 until the full-width exceeds 5 ns. The lesser sensitivity of χ^2_R to the Gaussian full-width is a reflection of the more rapid decrease of $\alpha(\tau)$ to zero as compared to the Lorentzian distribution (fig. 1). The results in fig. 3 seem to indicate that the full-widths of 1 ns or less can be only roughly determined from the frequency-domain data. In practice, the full-widths recovered from actual data have been narrower than the 1 ns limit implied by fig. 3. This favorable result is probably because for a true single-exponential decay the value of χ^2_R

decreases continually if the full-width is decreased.

The results are less favorable if we investigate whether a unimodal distribution can be distinguished from a double-exponential decay. When analyzed using the double-exponential model the values of χ^2_R were near unity, even as the widths were increased to 12 ns. A similar result was found for a wide variety of experimental data. In numerous cases we tried to obtain proof for the presence of distributions. Almost invariably, we found that the values of χ^2_R for the suspected distribution were the same as that found using a sum of exponentials with one more component.

A similar series of simulations were performed for bimodal distributions with mean lifetimes of 5 and 15 ns (fig. 3, right). In this case the widths needed to exceed 2–4 ns for the decay to be distinguished from the double-exponential model. It would not be possible to distinguish the bimodal distribution from a triple-exponential model, as can be judged from the values of χ^2_R which are near unity for widths as large as 12 ns.

4.3. Resolution of lifetime-distribution parameters

Suppose we know that the decay is due to a unimodal or a bimodal distribution. It is of interest to determine whether the parameters describing the distribution can be recovered from the data. This was done by examination of the χ^2_R surfaces for fixed values of either the full-width (fig. 4) or the mean decay times (fig. 5). Unimodal (left) and bimodal (right) data were simulated with full-widths of 5 ns. The simulated data were analyzed with one parameter value held fixed at values bracketing the correct values. Then, least-squares analysis is used to find the minimum value of χ^2_R. During this process the other floating parameters vary to compensate for the incorrectness of the fixed parameter. If the value of χ^2_R is elevated, then the fixed-parameter value is unacceptable. If χ^2_R is not elevated then the data cannot exclude the fixed-parameter value. The steepness of the χ^2_R surface for the parameter indicates the certainty with which the data determine its value. The relative increase in χ^2_R can be used to determine the uncertainties in the parameters. This procedure takes into account correlation between the parameters, and probably overestimates the uncertainties in the parameters.

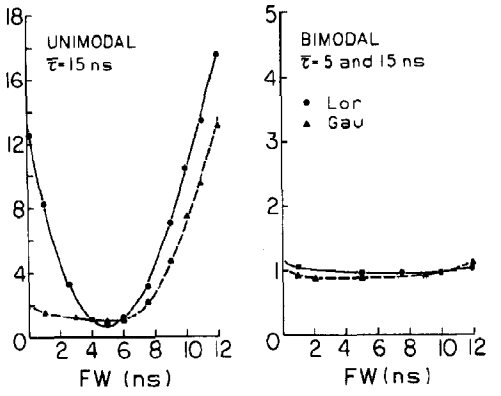

Fig. 4. Dependence of χ^2_R on the full-width of lifetime distributions. (Left) Values used for simulation: $\bar{\tau}=15$ ns and fw = 5 ns. Lorentzian (●———●), Gaussian (▲———▲). The simulated data were analyzed using the fw indicated on the x-axis. (Right) Values used for simulation: $\bar{\tau}_1=5$, $\bar{\tau}_2=15$, $fw_1=fw_2=5$ ns, $f_1=f_2=0.5$. Only one full-width was held constant (fw_1), and the second was varied during the χ^2_R minimization.

The results of this analysis are quite favorable for the one-component model, especially for the Lorentzian distribution (fig. 4). In this case, χ^2_R rises quickly to become unacceptable if the full-width is held below 4 or above 6 ns. The Gaussian displayed less sensitivity, especially for smaller full-widths. Nonetheless, the χ^2_R values do show reasonable minima near the correct full-width. The sensitivity of χ^2_R to the full-width is considerably weaker for the bimodal distribution. Full-widths ranging from 0 to 12 ns resulted in only a 10% change in χ^2_R. Hence, at the current levels of precision, using data from a single measurement, the full-widths of bimodal distributions are not likely to be reliably determined. However, we were able to recover reasonable full-widths from bimodal distributions for single-tryptophan proteins (see below). Apparently, even the weak χ^2_R dependence in fig. 4 can reveal the half-widths.

We also examined the sensitivity of χ^2_R to the mean lifetimes of the distributions. For a unimodal distribution (fig. 5, left) the values of χ^2_R are strongly dependent on $\bar{\tau}$, indicating that the mean values are easily determined. A similar

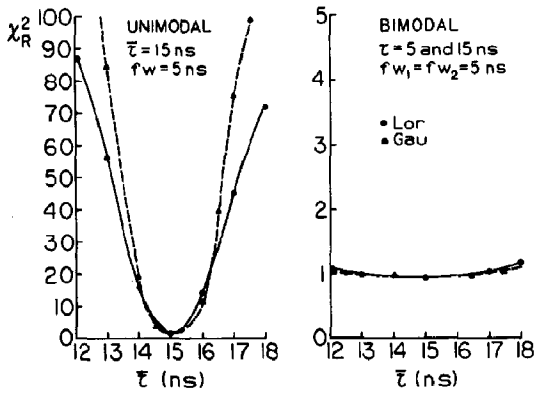

Fig. 5. Sensitivity of χ^2_R to the mean decay times of the distribution. Same as fig. 4 except the $\bar{\tau}_i$ values were held fixed during χ^2_R minimization.

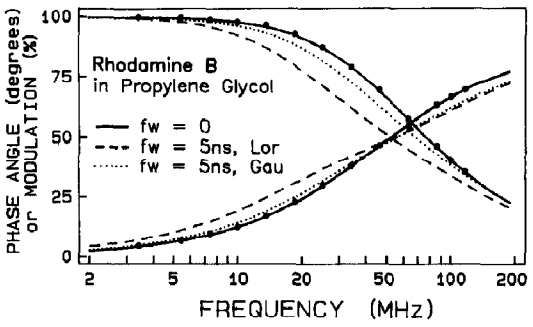

Fig. 6. Frequency-dependent phase and modulation data for rhodamine B in propylene glycol at −5°C. The excitation wavelength was 442 nm from an HeCd laser, and the emission was observed through a Corning 3-71 filter using magic-angle polarizer orientation. (———) Best Lorentzian (fw = 0.003) and best Gaussian (fw = 0.01) fits to the data (●). (— — —) Best fit with the Lorentzian full-width held constant at 5 ns; χ^2_R = 542. (·····) Best fit to a Gaussian with the full-width held constant at 5 ns; χ^2_R = 109.

sensitivity to $\bar{\tau}$ was found whether the distribution was Lorentzian or Gaussian. Resolution of the correct lifetime appears to be more difficult for a bimodal distribution. In this case, χ^2_R increases only 10% for a 3 ns shift in the value of $\bar{\tau}_2$. Nonetheless, as the χ^2_R surface is well-behaved, the correct values may be recovered from the analysis.

4.4. Experimental data for a one-component sample; rhodamine B

It is of interest to analyze experimental data in terms of the lifetime distributions. As our first example we chose a single-component solution of rhodamine B. The frequency-domain data are shown in fig. 6. For both the Lorentzian and Gaussian models we obtained a narrow unimodal lifetime distribution (fig. 7). In fact, the narrowness of distributions was smaller than expected. Hence, we attempted to force-fit the data with a wider distribution. The results of a Lorentzian force-fit with a 5 ns full-width are shown in fig. 6 (— — —). The systematic deviations between the model and the data allowed this wide distribution to be rejected. Similarly, the data were not consistent with a 5 ns wide Gaussian distribution (·····). The dependence of χ^2_R on the widths of the distributions is shown as an inset to fig. 7. The value of χ^2_R rises quickly for a Lorentzian of 0.1 ns width or larger, while the value of χ^2_R for the Gaussian does not rise until the full-width exceeds 1.0 ns. Nonetheless, repeated analysis of the data with various starting values for the parameters, including large half-widths, consistently yielded the narrow distribution shown in fig. 7. Apparently, the χ^2_R surface does not contain local minima which would result in erratic values for the final parameters.

4.5. A two-component mixture of 9-MA and 9-CA

We examined mixtures of fluorophores, each of which was expected to decay as a single exponential. If the resolution is adequate we expect the analysis to reveal sharp distributions, similar to those indicated by the vertical bars in fig. 1. The two-component mixture contained 9-MA (4.4 ns) and 9-CA (12.1 ns). The frequency-domain data for a 50:50 (9-CA/9-MA) mixture are shown in fig. 8. It was not possible to fit the data to a unimodal Lorentzian (— — —, O). Of course, the data are in agreement with the double-exponential or the bimodal Lorentzian models.

The analysis of the 50:50 mixture of 9-CA and 9-MA is summarized in table 1. Surprisingly, we were able to recover rather narrow distributions for this two-component mixture (fig. 9). If the data are analyzed with a unimodal Lorentzian the

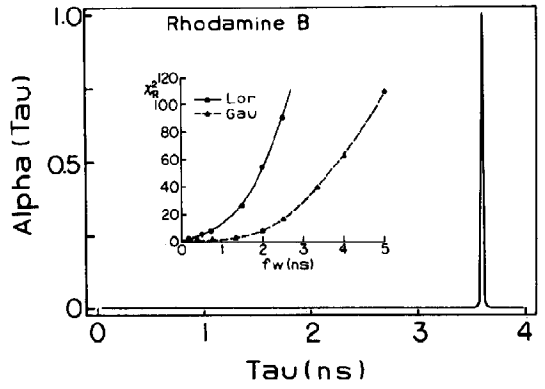

Fig. 7. Lifetime distribution for rhodamine B at −5°C. The intensity decay of rhodamine B is narrowly distributed near 3.6 ns. (Inset) Dependence of χ^2_R on the full-width when held at constant values.

apparent width is large (4.9 ns), and χ^2_R is not acceptable (12-fold larger than the minimum value). In contrast, the bimodal Lorentzian model yields an acceptable fit for the mixture, and correct values for the average lifetimes, which are in agreement with both the independently measured values and those recovered from the usual multi-exponential model (denoted by Het in table 1). Several points should be stressed. First, the apparent full-widths are quite small (0.24 and 0.13 ns). At present, we do not believe that these values should be accepted as precisely correct. There must be considerable uncertainty because the value of χ^2_R is similar for the double-exponential model with two less floating parameters. In fact, the lack of decrease in χ^2_R by the addition of these two floating parameters (fw_1 and fw_2) indicates that these parameters are not needed to account for the data. Secondly, the additional floating parameters in the distribution models result in greater difficulty in recovering acceptable parameter values. This is evident from the rather low value of χ^2_R for the unimodal Lorentzian ($\chi^2_R = 3.7$) as compared to the single-exponential decay model ($\chi^2_R = 110.8$, Het, 1 τ). Nonetheless, analysis of the experimental data for a mixture yielded sharp distributions (fig. 9). This is an important result because it demonstrates that the similar widths

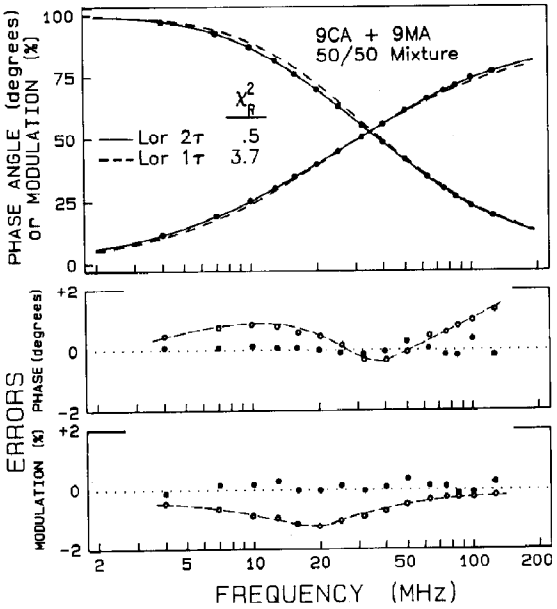

Fig. 8. Phase and modulation data for mixtures of 9-MA and 9-CA in ethanol. Data (●) are shown for a mixture with 50% of the emission from 9-CA ($f_1 = f_2 = 0.5$). Best fits are shown for a one-component Lorentzian (— — —) and a two-component Lorentzian (———). Deviations for the one- (○) and two-component (●) Lorentzians are shown in the lower panels.

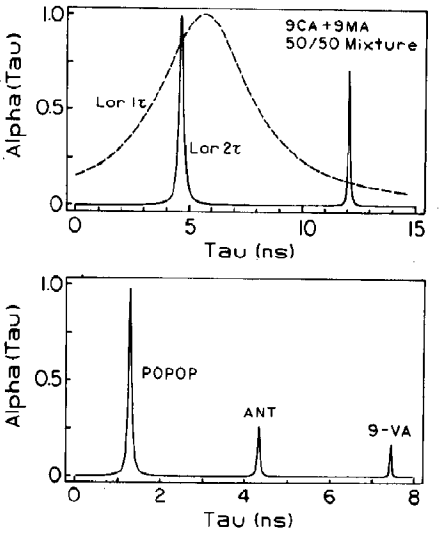

Fig. 9. Distribution of lifetimes recovered from two- and three-component mixtures. (Top) Two-component mixture of 9-CA and 9-MA from fig. 8. (———) Best two-component Lorentzian fit (table 1); (— — —) best one-component Lorentzian. (Bottom) Three-component mixture of POPOP, anthracene (ANT) and 9-VA. The results represent one profile from a global analysis using the three-component Lorentzian model (table 2).

Table 1

Analysis of two-component mixtures of 9-MA and 9-CA

Model	$\bar{\tau}_i$ (ns)	fw$_i$ (ns)	f_i	χ^2_R
50:50 mixture				
Het, 2 τ	4.6	–	0.51	0.5 [b]
	12.0	–	0.49	
Het, 1 τ	6.6	–	1.0	110.8
Lor, 2 τ	4.6	0.24	0.47	
	11.9	0.13	0.53	0.5
Lor, 1 τ	5.6	4.87	1.0	3.7
Gau, 1 τ	5.8	8.33	1.0	7.58
Gau, 2 τ	4.6	0.83	0.48	
	11.7	0.29	0.53	0.33
Five 9-MA/9-CA mixtures				
Het, 2 τ	4.5	–	0.11/0.28/0.51/0.77/0.91	0.43
	11.9			
Het, 1 τ	7.1	–	–	566
Expected f_1 values	–	–	0.1/0.25/0.50/0.75/0.90	–
Lor, 1 τ	5.9	3.88	–	504
Lor, 2 τ	4.4	0.14	0.07/0.22/0.48/0.72/0.89	
	11.9	0.21		0.45
Gau, 1 τ	6.2	7.18	–	506
Gau, 2 τ	4.5	0.25	0.09/0.24/0.49/0.73/0.89	
	11.9	2.05		0.44

[a] The independently measured lifetimes of 9-MA and 9-CA are 4.4 and 12.1 ns, respectively. The excitation wavelength was 325 nm from an HeCd laser, the emission being observed through a Corning cut-off filter.

[b] $\delta\phi = 0.2°$, $\delta m = 0.005$.

observed for other samples are not the result of lack of resolution of the data.

The greater complexity of the lifetime-distribution models can be partially overcome by the use of global methods. We measured and analyzed data from five mixtures of 9-MA and 9-CA, with $f_1 = 0.1$, 0.25, 0.50, 0.75 and 0.90. For this case there is a 1000-fold decrease in χ^2_R from the unimodal ($\chi^2_R = 504$) to the bimodal ($\chi^2_R = 0.45$) Lorentzian, as compared with the 12-fold decrease when a nonglobal analysis is performed. The recovered lifetime distribution closely approximates the expected δ-functions. Additionally, the integrated α_i values for each mixture agreed with the expected values (table 1).

These data were also analyzed using Gaussian distributions. For these particular solutions the unimodal Lorentzian and Gaussian models were equally successful in accounting for the data. The apparent widths recovered using the bimodal Gaussian model were about 4-fold larger than for the Lorentzian.

4.6. Analysis of a three-component mixture

We examined three-component mixtures of POPOP, anthracene and 9-VA. We were surprised to find that χ^2_R decreased 40-fold for the trimodal Lorentzian as compared with the bimodal Lorentzian (table 2). Attempts to fit the data to the simpler models (unimodal or bimodal) resulted in wide full-widths and unacceptable values of χ^2_R. For the trimodal Lorentzian the integrated intensities were in good agreement with those expected from the known proportions in the mixtures. Remarkably, these distributions closely approximate the δ-function distribution expected for a mixture of exponentially decaying fluorophores (fig. 9).

4.7. Closely spaced decay times

It must be emphasized that an ability to fit the data to a unimodal distribution does not demon-

Table 2

Global [a] analysis of three-component mixtures of POPOP, anthracene and 9-VA

Model	$\bar{\tau}_i$ (ns)	fw$_i$ (ns)	f_i	χ^2_R
Het, 3 τ	1.3	–	0.25/0.41/0.16	
	4.2	–	0.22/0.35/0.49	
	7.5	–	0.53/0.24/0.35	0.24
Het, 2 τ	1.4	–	–	9.8
	6.0	–	–	
Het, 1 τ	3.3	–	–	666
Lor, 3 τ	1.3	0.07	0.25/0.41/0.16	
	4.3	0.06	0.22/0.35/0.49	
	7.4	0.03	0.53/0.24/0.35	0.25
Lor, 2 τ	1.2	0.03	–	
	4.9	1.79	–	10.9
Lor, 1 τ	1.5	3.13	–	231
Expected f_i values			3/5/2	
			2/3/5	
			5/2/3	

[a] The data from three files were analyzed simultaneously. The fractional intensities recovered from both three-component fits (Lor and Het) agreed with the expected values.

[b] $\delta\phi = 0.2°$, $\delta m = 0.005$.

strate that the decay is due to a unimodal lifetime distribution. The possibility of incorrectly accepting a unimodal distribution is illustrated in table 3, which shows the results of analyzing data due to two closely spaced decay times (anthracene, 4.0 ns and diphenylanthracene, 6.3 ns). For this sample we believe that the decay is in fact a double exponential. However, the data are fitted equally well using the unimodal Lorentzian or Gaussian models. Hence, as the decays become more closely spaced, it will not be possible to determine the actual form of the decay law.

4.8. Decay-time distribution for an excited-state reaction

One application of the distribution analysis is for excited-state processes. Such systems display complex wavelength-dependent decay kinetics, and the nonexponential behavior of some systems should result in broadly distributed lifetimes. For the initial analysis we selected the excited-state deprotonation of 2-naphthol [27]. It is known that the pK_a of naphthol is 9.2 in the ground state, and that it decreases to 2.0 in the excited state. The loss of a proton competes with emission, and the pH and reaction rates determine the relative emission from naphthol and naphtholate. At pH 7 the reaction is irreversible, whereas reprotonation can occur at pH 3. The reaction scheme contains only two excited states, naphthol and naphtholate, so that at each wavelength the decay is described by a double-exponential decay. Since the emission from each species is distinct (fig. 10, inset) the chosen emission wavelengths affect the relative contribution of each species to the phase and

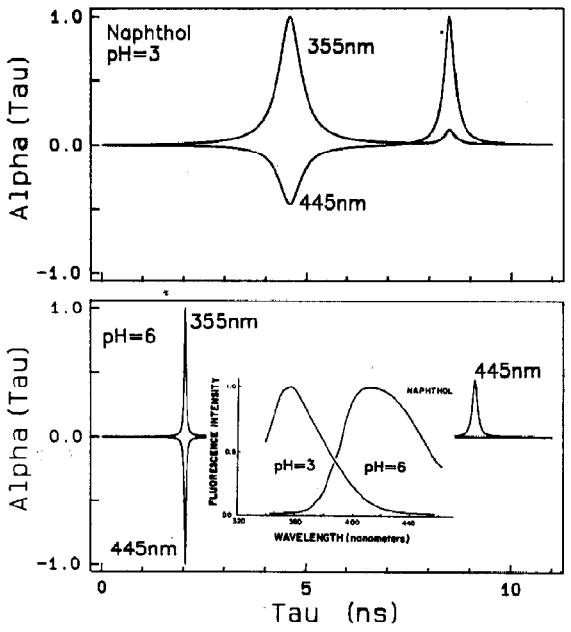

Fig. 10. Distribution of decay times for naphthol of pH 3 (top) and pH 6 (bottom). (Inset) Emission spectra of naphthol and naphtholate. The decay-time distributions are shown at 355 and 445 nm. These were recovered by global analysis of data measured at nine wavelengths from 340 to 460 nm. Data from ref. 34.

modulation data. One interesting feature of this system is that the preexponential factors can be negative for the reaction product. The intensity decay of naphtholate is expected to display equal and opposite preexponential factors. Additionally, the intensity decay of naphthol is known to be a single exponential if the reaction is irreversible (pH 6) and to be a double exponential if the reaction is reversible (pH 3).

We analyzed previously obtained data for naphthol at nine emission wavelengths [34]. These data were analyzed globally, resulting in the distributions shown in fig. 10. The data for 355 nm are due to emission from naphthol, and those for 445 nm to emission from naphtholate. The α values are sharply distributed, and reflect the reversibility of the reaction. On the blue side of the emission (355 nm) the α distribution is bimodal at pH 3, and unimodal at pH 6, indicating double- and single-exponential decays, respectively. While the bimodal character at 355 nm and pH 3 is weak,

Table 3

Distribution analysis of a mixture of anthracene and diphenylanthracene

Model	$\bar{\tau}$ (ns)	f_i or fw (ns)	χ^2_R
Het, 1 τ	5.13	1.00	6.14 [a]
Het, 2 τ	3.92	0.37	0.13
	6.17	0.63	0.13
Gau, 1 τ	5.08	2.69	0.13
Lor, 1 τ	5.05	1.05	0.16

the decay at 355 nm is unambiguously a multiexponential. It is known that a reversible process yields a doubly-exponential decay law for the initially excited species, whereas for an irreversible reaction this species decays as a single exponential. On the red side of the emission (445 nm) the distributions show regions of negative intensity. This is expected for the product of an excited-state process. At present, we do not know whether the wider distributions found at pH 3 are a consequence of the reversibility of the reactions or are due to experimental uncertainties in the full-widths.

4.9. *Effects of time-dependent spectral relaxation*

It is known that time-dependent reorganization of polar molecules around an excited fluorophore can yield nonexponential decays [17]. In the presence of solvent relaxation the intensity decays are known to be highly dependent on emission wavelength, which is a consequence of a continuous time-dependent shift towards longer wavelengths. We used the data described previously [39] to recover the wavelength-dependent lifetime distributions for TNS-labeled vesicles of DOPC (fig. 11). The α distributions show regions of both positive and negative intensity, as is expected for an excited-state process. Significantly, the distributions are rather broad at low temperatures (top), becoming sharper at higher temperatures (bottom). This is an important observation because it indicates that broadly distributed α values can be the result of local interactions with surrounding groups, and depend upon the rate at which these interactions reach equilibrium. We believe that the α distributions will prove to be generally useful as an indicator of the dynamics of the environment surrounding fluorophores in macromolecules. Two laboratories have already reported that the intrinsic tryptophan emission from proteins become more sharply distributed at higher temperatures [9,40].

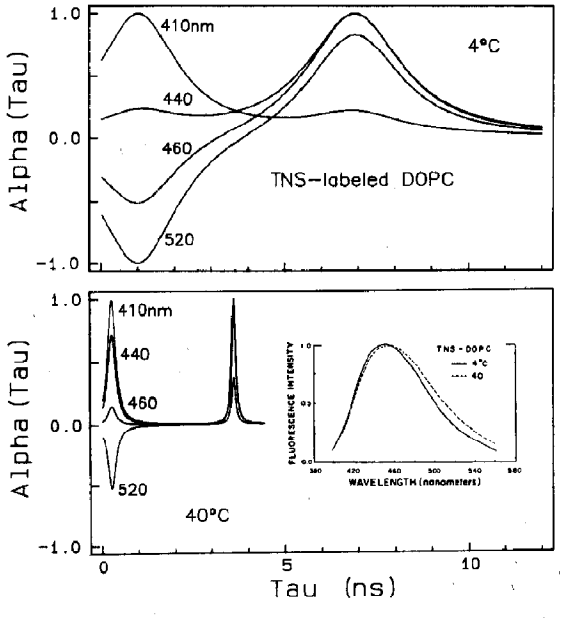

Fig. 11. Wavelength-resolved decay-time distribution of TNS-labeled DOPC vesicles, at 4°C (top) and 40°C (bottom). (Inset) Emission spectra at 4 and 40°C.

4.10. *Transient effects in collisional quenching*

A variety of processes can result in nonexponential decays of fluorescence. One common example is collisional quenching of fluorescence. An initially single-exponential decay can become

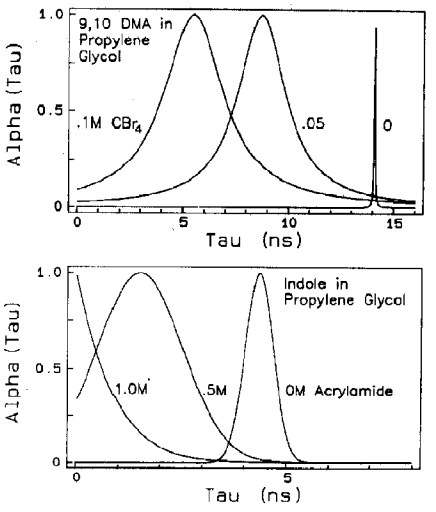

Fig. 12. Lifetime distributions resulting from transient effects in quenching. (Top) Data are for 9,10-DMA quenched by carbon tetrabromide in propylene glycol at 25°C. (Bottom) Data are for indole in propylene glycol at 20°C quenched by 0, 0.5, and 1.0 M acrylamide [41].

nonexponential in the presence of quenching [19–22]. This occurs because of the initial random distribution of the fluorophore-quencher pairs in homogeneous solution. Following light absorption the more closely spaced pairs are rapidly quenched, resulting in a slower decay at longer times due to the more widely spaced pairs. Interpretation of these decays in terms of the molecular features of the systems is complex. Nonetheless, the quenching-induced heterogeneity can be visualized from the decay-time distribution. This is illustrated in fig. 12 for benzanthracene quenched by carbon tetrabromide and for indole quenched by acrylamide [41]. In both cases quenching causes the distribution to become wider and shift towards shorter decay times. Visualization of such distributions for either the decay time or the rates of quenching should be valuable for evaluating the molecular details of quenching of macromolecules.

4.11. Energy transfer and distance distributions

Fluorescence energy transfer can also result in a distribution of decay times. If the donor and acceptor are at a fixed distance then the decay of the donor is shortened by transfer, but the decay will remain a single exponential. However, if a range of donor-acceptor distances are present, then these will exist in a range of transfer rates, and hence a range of decay times. This is illustrated in fig. 13 for tryptamine linked to a dansyl group via a flexible chain. In the absence of acceptor the decay of tryptamine is predominately a single exponential. In the presence of acceptor the donor decay is shortened, and now exhibits a range of decay times. If there were two unique distances then we would expect a bimodal distribution. Since this was not observed we believe that a continuous range of donor-acceptor distances is accessible to this molecule. While data for this donor-acceptor pair can be analyzed using a decay-time distribution, we believe it is preferable to formulate the analysis in terms of parameters which characterize the distribution of distances [25].

4.12. Single-tryptophan proteins

As a final example of decay-time distributions we describe the results for indole in water and for several single-tryptophan proteins. For indole in water the decay-time distribution appears to become sharper at higher temperatures (fig. 14, top). This decrease in width is also apparent from the values of χ_R^2 resulting from the distribution analysis. At low temperature (5 °C) the value of χ_R^2

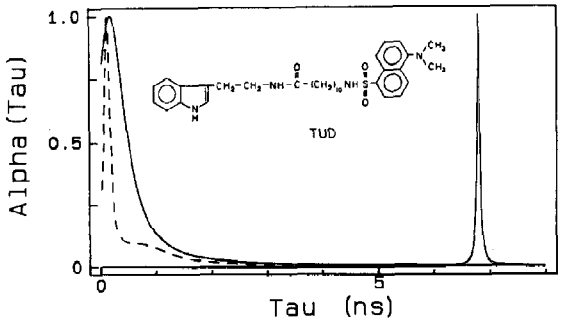

Fig. 13. Lifetime distribution resulting from energy transfer with a range of donor-to-acceptor distances. Data are for tryptamine linked to dansylundecanoic acid (TUD) [25], and were analyzed using the uni- (———, left) and bimodal (— — —) Lorentzians. The solid line to the right is for donor in the absence of acceptor, tryptamine-myristic acid.

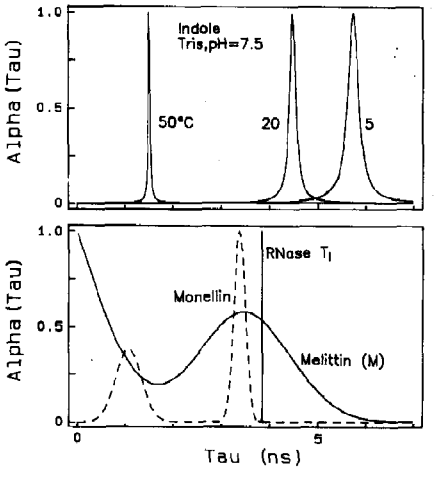

Fig. 14. Lifetime distributions of single tryptophan proteins. (Top) Distribution for the intensity decay of indole in water at various temperatures. (Bottom) Decay-time distributions for monellin (— — —), melittin monomer (———) and RNase T_1 (vertical line).

Table 4

Multiexponential and distribution analysis for indole in water [a]

Temperature (°C)	Model	τ_i (ns)	fw_i (ns)	α_i	χ^2_R
5	Het, 1 τ	5.72	–	1.0	1.3
	Het, 2 τ	3.62	–	0.07	
		5.87	–	0.93	1.1
	Lor, 1 τ	5.72	0.26	1.0	1.0
	Gau, 1 τ	5.72	1.43	1.0	1.0
20	Het, 1 τ	4.49	–	1.0	1.9
	Het, 2 τ	2.90	–	0.06	
		4.58	–	0.94	1.7
	Lor, 1 τ	4.48	0.15	1.0	1.6
	Gau, 1 τ	4.49	1.08	1.0	1.6
50	Het, 1 τ	1.52	–	1.0	2.5
	Het, 2 τ	0.65	–	0.04	
		1.55	–	0.94	2.2
	Lor, 1 τ	1.51	0.04	1.0	2.3
	Gau, 1 τ	1.52	0.40	1.0	2.2

[a] 0.025 M Tris, pH 7.5.

decreases for the unimodal models, relative to the single-exponential fits (table 4). At higher temperature (20 and 50 °C) the decrease in χ^2_R becomes smaller, which reflects the sharper distribution. This effect may be due to increased dynamic homogeneity at higher temperatures.

The emission from the single-tryptophan proteins is of interest because it may be possible to interpret the results in terms of structural and dynamic features of the proteins. We have noticed that the distributions vary widely among single-tryptophan proteins, which may reflect the diverse

Table 5

Multiexponential and distribution analysis for single-tryptophan proteins

Protein	Model	$\bar{\tau}_i$ (ns)	fw_i (ns)	α_i	χ^2_R
RNase T_1 [a]	Het, 1 τ	3.83	–	1.0	0.83
	Gau, 1 τ	3.83	0.0004	1.0	0.85
	Lor, 1 τ	3.83	0.04	1.0	0.93
Melittin monomer [b]	Het, 2 τ	0.88	–	0.36	
		3.72	–	0.64	2.8
	Gau, 2 τ	−1.13	2.82	0.37	
		3.47	2.23	0.63	1.5
	Het, 3 τ	0.24	–	0.32	
		2.12	–	0.33	
		4.22	–	0.36	1.2
Monellin [c]	Het, 2 τ	1.01	–	0.43	
		3.31		0.57	1.0
	Gau, 2 τ	1.07	0.63	0.46	
		3.38	0.28	0.54	1.05

[a] 100 mM sodium acetate, pH 5.5, 20 °C.
[b] 10 mM Tris, pH 7.0, 20 °C.
[c] 25 mM Tris, 100 mM NaCl, pH 7.0, 20 °C.

environments which surround tryptophan residues in different proteins. The single tryptophan residue of RNase T_1 is known to be highly shielded from the aqueous phase [42] and is located in the interior of the protein [43]. In this case, the decay was found to be a single exponential, in agreement with other time-resolved studies of this protein [44]. Data for RNase T_1 and the other proteins were from ref. 45. The fit to the RNase T_1 data could not be improved using a double-exponential model or the unimodal distributions (table 5). It should be noted that these measurements were at pH 5.5, and the decays may be more complex at other pH values (M.R. Eftink, personal communication).

In contrast to RNase T_1, the intensity decay of melittin monomer is highly heterogeneous. While the double-exponential model (Het, 2 τ) provides a reasonable fit to the data ($\chi^2_R = 2.8$), the value of χ^2_R decreases 2.3-fold for a triple-exponential analysis (Het, 3 τ, table 5). The bimodal Gaussian provides a good fit to the data ($\chi^2_R = 1.5$), and suggests a broad distribution of decay times with significant α density near $\tau = 0$. This distribution is in rough agreement with the triple-exponential model which yielded a decay time near 0.24 ns. In solution, monomeric melittin is mostly in the random-coil state. It is possible that the decay-time distribution reflects the range of environments experienced by the tryptophan residue. Indeed, the sharp distribution found for RNase T_1 may reflect the uniformity of the environment surrounding the tryptophan residue. A uniform environment is not expected for monomeric melittin.

The decay-time distribution for monellin is intermediate between that found for RNase T_1 and melittin (fig. 14). The distribution appears to be bimodal, with widths near 0.5 ns. In contrast to melittin, the values of χ^2_R do not support acceptance of the distribution model (table 4). Monellin probably adopts a single conformation in solution, which may be the origin of the bimodal distribution seen in fig. 14. Additional experimentation and analysis are required to evaluate the correlation, if any, between protein structure and the decay-time distributions.

5. Conclusions

Analysis of fluorescence decay kinetics in terms of distributions is still in its infancy. A variety of phenomena can result in decay-time distributions, and it seems likely that the distribution models will become widely utilized. At present, it is difficult to distinguish distributions from multiexponential decays. To some extent this difficulty can be overcome by global experimentation and analysis. Except for favorable circumstances, it seems unlikely that distinction between these similar models can be unambiguous with data available in the foreseeable future. For this reason it will be necessary to regard the distribution and the multiexponential models as alternative presentations, and to select the appropriate model using other known properties of the samples.

Acknowledgements

The authors thank Susan Frasier for her thoughtful suggestions for improving the manuscript. Supported by grants from the National Institutes of Health (GM 35154) and from the National Science Foundation (DMB-8502835 and DMB-8511065).

References

1 A. Grinvald and I.Z. Steinberg, Anal. Biochim. 59 (1974) 583.
2 D.V. O'Connor, W.R. Ware and J.C. Andre, J. Phys. Chem. 83 (1979) 1333.
3 J.N. Demas, Excited state lifetime measurements (Academic Press, New York, 1983).
4 D.V. O'Connor and D. Phillips, Time-correlated single photon counting (Academic Press, New York, 1984).
5 D.R. James and W.R. Ware, Chem. Phys. Lett. 120 (1985) 455.
6 D.R. James, Y.S. Liu, P. DeMayo and W.R. Ware, Chem. Phys. Lett. 120 (1985) 460.
7 D.R. James and W.R. Ware, Chem. Phys. Lett. 126 (1986) 7.
8 J.R. Alcala, E. Gratton and F.G. Prendergast, Biophys. J. 51 (1987) 587.
9 J.R. Allcala, E. Gratton and F.G. Prendergast, Biophys. J. 51 (1987) 597.
10 J.R. Allcala, E. Gratton and F.G. Prendergast, Biophys. J. 51 (1987) 925.

11 W.R. Ware, L.J. Doemeny and T.L. Nemzek, J. Phys. Chem. 77 (1973) 2038.
12 A. van Hoek, J. Vervoost and A.J.W.G. Visser, J. Biochem. Biophys. Methods 7 (1983) 243.
13 E.W. Small, L.J. Libertini and I. Isenberg, Rev. Sci. Instrum. 55 (1984) 879.
14 E. Gratton and M. Limkemann, Biophys. J. 44 (1983) 315.
15 J.R. Lakowicz and B.P. Maliwal, Biophys. Chem. 21 (1985) 61.
16 J.R. Lakowicz, G. Laczko and I. Gryczynski, Rev. Sci. Instrum. 57 (1986) 2499.
17 N.G. Bakhshiev, Y.T. Mazurenko and I.V. Peterskaya, Opt. Spectrosc. 21 (1966) 307.
18 J.R. Lakowicz, Principles of fluorescence spectroscopy (Plenum Press, New York, 1983).
19 F.C. Collins and G.E. Kimball, J. Colloid Sci. 4 (1949) 425.
20 T.L. Nemzek and W.R. Ware, J. Chem. Phys. 62 (1975) 477.
21 J.R. Lakowicz, M.L. Johnson, N. Joshi, I. Gryczynski and G. Laczko, Chem. Phys. Lett. 131 (1986) 343.
22 N. Joshi, M.L. Johnson, I. Gryczynski and J.R. Lakowicz, Chem. Phys. Lett. 135 (1987) 200.
23 R.G. Bennet, J. Chem. Phys. 41 (1964) 3037.
24 B.K.K. Fung and L. Stryer, Biochemistry 17 (1978) 5241.
25 J.R. Lakowicz, M. Johnson, W. Wiczk, A. Bhat and R.F. Steiner, Chem. Phys. Lett. (1987) in the press.
26 P.R. Bevington, Data reduction and error analysis for the physical sciences (McGraw-Hill, New York, 1969).
27 W.R. Laws and L. Brand, J. Phys. Chem. 83 (1979) 795.
28 H.J. Galla and W. Hartmann, Chem. Phys. Lipids 27 (1980) 199.
29 R.P. DeToma, J.H. Easter and L. Brand, J. Am. Chem. Soc. 98 (1976) 5001.
30 W.R. Ware, S.K. Lee, G.J. Brant and P.P. Chow, J. Chem. Phys. 54 (1970) 4729.
31 J.R. Lakowicz and A. Balter, Biophys. Chem. 16 (1982) 223.
32 J.R. Lakowicz and A. Balter, Biophys. Chem. 16 (1982) 99.
33 J.R. Lakowicz and A. Balter, Biophys. Chem. 16 (1982) 117.
34 J.R. Lakowicz and H. Cherek, Chem. Phys. Lett. 122 (1985) 380.
35 J.R. Lakowicz, E. Gratton, G. Laczko, H. Cherek and M. Limkemann, Biophys. J. 46 (1984) 463.
36 E. Gratton, J.R. Lakowicz, B. Maliwal, H. Cherek, G. Laczko and M. Limkemann, Biophys. J. 46 (1984) 479.
37 J.R. Knutson, J.M. Beechem and L. Brand, Chem. Phys. Lett. 102 (1983) 501.
38 M.L. Johnson, Biophys. J. 44 (1983) 101.
39 J.R. Lakowicz, H. Cherek, G. Laczko and E. Gratton, Biochim. Biophys. Acta 777 (1984) 183.
40 H. Cherek, I. Gryczynski, G. Laczko, M.L. Johnson and J.R. Lakowicz, International symposium on molecular luminescence and photophysics (Torun, Poland, 1986) p. 71.
41 J.R. Lakowicz, M.L. Johnson, I. Gryczynski, N. Joshi and G. Laczko, Biophys. J. 51 (1987) 755.
42 M.R. Eftink and C.A. Ghiron, Biochemistry 15 (1976) 672.
43 H. Heinemann and W. Saenger, Nature 279 (1982) 27.
44 D.R. James, D.R. Dremmer, R.P. Steer and R.E. Verrat, Biochemistry 24 (1985) 5517.
45 J.R. Lakowicz, I. Gryczynski, H. Szmacinski, H. Cherek and N. Joshi, (1987) submitted for publication.